ACS APPLIED MATERIALS & INTERFACES

www.acsami.org

Research Article

Theoretical Design of Lithium Chloride Superionic Conductors for All-Solid-State High-Voltage Lithium-Ion Batteries

Dongsu Park, Haesun Park, Yongheum Lee, Sang-Ok Kim, Hun-Gi Jung, Kyung Yoon Chung, Joon Hyung Shim, and Seungho Yu*

Cite This: *ACS Appl. Mater. Interfaces* 2020, 12, 34806–34814

Read Online

ACCESS | Metrics & More | Article Recommendations | Supporting Information

ABSTRACT: The development of solid electrolytes (SEs) is a promising pathway to improve the energy density and safety of conventional Li-ion batteries. Several lithium chloride SEs, Li_3MCl_6 (M = Y, Er, In, and Sc), have gained popularity due to their high ionic conductivity, wide electrochemical window, and good chemical stability. This study systematically investigated 17 Li_3MCl_6 SEs to identify novel and promising lithium chloride SEs. Calculation results revealed that 12 Li_3MCl_6 (M = Bi, Dy, Er, Ho, In, Lu, Sc, Sm, Tb, Tl, Tm, and Y) were stable phase with a wide electrochemical stability window and excellent chemical stability against cathode materials and moisture. Li-ion transport properties were examined using bond valence site energy (BVSE) and *ab initio* molecular dynamics (AIMD) calculation. Li_3MCl_6 showed the lower migration energy barrier in monoclinic structures, while orthorhombic and trigonal structures exhibited higher energy barriers due to the sluggish diffusion along the two-dimensional path based on the BVSE model. AIMD results confirmed the slower ion migration along the 2D path, exhibiting lower ionic diffusivity and higher activation energy in orthorhombic and trigonal structures. For the further increase of ionic conductivity in monoclinic structures, Li-ion vacancy was formed by the substitution of M^{3+} with Zr^{4+}. Zr-substituted phase ($Li_{2.5}M_{0.5}Zr_{0.5}Cl_6$, M = In, Sc) exhibited up to a fourfold increase in ionic conductivity. This finding suggested that the optimization of Li vacancy in the Li_3MCl_6 SEs could lead to superionic Li_3MCl_6 SEs.

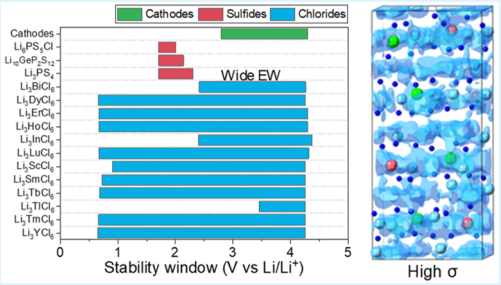

KEYWORDS: *energy storage, all-solid-state batteries, solid electrolytes, chloride solid electrolytes, materials design*

1. INTRODUCTION

Lithium-ion batteries are widely used in portable electronics and have become popular candidates in emerging applications that specifically demand high energy density and enhanced safety, including electric vehicles and energy storage systems.[1,2] One promising pathway is the development of solid electrolytes (SEs).[3−5] SEs with a metallic Li anode exhibit higher energy density than conventional graphite-based anodes,[6] which allow the high energy density of Li−S and Li−air batteries.[7,8] Furthermore, SEs significantly improve safety by replacing the flammable conventional liquid electrolytes.[9]

Various types of SEs have been applied in all-solid-state lithium batteries.[10−12] Sulfide SEs exhibit a high ionic conductivity (10 mS/cm), which is comparable to that of liquid electrolytes.[12,13] However, sulfide SEs are unstable when exposed to moisture and exhibit narrow electrochemical stability.[14,15] Oxide SEs are chemically stable and show high ionic conductivity (~1 mS/cm for $Li_7La_3Zr_2O_{12}$)[16,17] but require a high-temperature sintering process.[18,19] Several lithium chloride SEs have been recently reported as promising SEs due to their high ionic conductivity, wide electrochemical window, chemical stability, and scalable synthesis.[20,21]

Asano et al. reported Li_3YCl_6 SEs with high ionic conductivity of 0.5 mS/cm,[22] and Li_3MCl_6 SEs (M = Er, In) have been subsequently developed.[23−26] Specifically, Li_3InCl_6 exhibited high ionic conductivity (2 mS/cm) and was synthesized by a scalable water-mediated method.[26] A recent study demonstrated the excellent ionic conductivity of Li_3ScCl_6 (3 mS/cm) at room temperature.[27] A theoretical study by Wang et al. reported that high ionic conductivity (~10 mS/cm) and good electrochemical stability is expected in Li chloride SEs.[20] Furthermore, Park et al. produced mixed-metal chlorides, namely, $Li_{3-x}M_{1-x}Zr_xCl_6$ (M = Y, Er), by replacing Y and Er with Zr. The resulting Li vacancy site in Li_3MCl_6 led to phase transition and increased ionic conductivity of up to 1.4 mS/cm.[28]

Although Li_3MCl_6 is a promising group of SEs, their development is still in the early stages.[21] This study aimed to systematically investigate 17 Li_3MCl_6 (M = Al, Bi, Dy, Er, Ga, Ho, In, La, Lu, Nd, Sb, Sc, Sm, Tb, Tl, Tm, and Y) to identify the promising compounds. The Li_3MCl_6 SEs were evaluated

Received: April 16, 2020
Accepted: July 9, 2020
Published: July 9, 2020

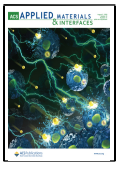

https://dx.doi.org/10.1021/acsami.0c07003
ACS Appl. Mater. Interfaces 2020, 12, 34806−34814

Table 1. Phase Stability (Energy above the Hull, E_{hull}, and Decomposition Phases) of Li_3MCl_6 SEs Based on the Space Group[43]

	E_{hull} (meV/atom)				
Li_3MCl_6	monoclinic (*C*2)	trigonal (*P*321)	orthorhombic ($Pna2_1$)	stability	decomp. phases
Li_3AlCl_6	25	64	46	unstable	$LiAlCl_4$, LiCl
Li_3BiCl_6	0	2	7	stable	N/A
Li_3DyCl_6	5	11	6	metastable	$DyCl_3$, LiCl
Li_3ErCl_6	0	0	0	stable	N/A
Li_3GaCl_6	45	82	64	unstable	$LiGaCl_4$, LiCl
Li_3HoCl_6	0	0	0	stable	N/A
Li_3InCl_6	0	0	0	stable	N/A
Li_3LaCl_6	55	51	51	unstable	$LaCl_3$, LiCl
Li_3LuCl_6	0	0	0	stable	N/A
Li_3NdCl_6	44	41	71	unstable	$NdCl_3$, LiCl
Li_3SbCl_6	26	38	32	unstable	$SbCl_3$, LiCl
Li_3ScCl_6	11	30	20	metastable	$ScCl_3$, LiCl
Li_3SmCl_6	6	7	4	metastable	$SmCl_3$, LiCl
Li_3TbCl_6	12	17	13	metastable	$TbCl_3$, LiCl
Li_3TlCl_6	17	31	21	metastable	$TlCl_3$, LiCl
Li_3TmCl_6	0	8	4	stable	N/A
Li_3YCl_6	20	25	21	metastable	YCl_3, LiCl

according to their electrochemical stability window, chemical stability against cathode materials and moisture, Li-ion migration pathway, and ionic conductivity. The effect of Li vacancy by aliovalent substitution on Li-ion migration was also investigated to improve the ionic conductivity.

Calculation results revealed that 12 Li_3MCl_6 (M = Bi, Dy, Er, Ho, In, Lu, Sc, Sm, Tb, Tl, Tm, and Y) were stable phases with a wide electrochemical stability window and good chemical stability against cathode materials and moisture. Li-ion transport properties examined by the bond valence site energy (BVSE) and *ab initio* molecular dynamics (AIMD) indicated that Li-ion migration was dependent on the structure of Li_3MCl_6. Most Li_3MCl_6 showed the lowest migration energy barrier in monoclinic structures, while orthorhombic structures and trigonal structures exhibited higher energy barriers. AIMD simulations showed that Li-ion migration through the 2D path along the *ab*-plane exhibited lower ionic diffusivity and higher activation energy in orthorhombic and trigonal structures. Based on the calculation results, monoclinic Li_3InCl_6 and Li_3ScCl_6 structures exhibit the highest ionic conductivities among Li_3MCl_6 SEs. For the further increase of ionic conductivity, Li-ion vacancy was formed by the aliovalent substitution of M^{3+} with Zr^{4+} in Li_3MCl_6 SEs. Zr-substituted phase $Li_{2.5}In_{0.5}Zr_{0.5}Cl_6$ and $Li_{2.5}Sc_{0.5}Zr_{0.5}Cl_6$ increased ionic conductivity up to fourfold at 300 K. This finding suggested that the optimization of substitution (type and level of Li vacancy) in the Li_3MCl_6 SEs would be helpful in developing superionic Li chloride SEs.

2. METHODS

First-principles calculations were performed based on a plane wave basis set, the projector augmented wave method,[29] and the generalized gradient approximation in the Perdew–Burke–Ernzerhof exchange–correlation functional[30] as implemented the Vienna *ab initio* simulation package.[31,32] The cutoff energy for the plane waves and *k*-points grid for the total energy calculations were consistent with the setting in the Materials Project (MP) database.[33] Energy corrections for anions, transition metals, and gas/liquid phases were included in the MP.[34,35]

The phase stability of the Li chlorides was evaluated based on Li–M–Cl phase diagrams from the MP.[36] The energy above the convex hull (E_{hull}) for the Li chlorides indicated the energy above the competing stable phases. The Li_3MCl_6 phases exhibiting E_{hull} below 25 meV/atom were considered as stable phases since they can be stabilized by entropic effects at room temperature. The electrochemical stability of the Li chlorides was determined using the grand potential phase diagram as a function of the chemical potential of Li

$$\mu_{Li}(\varphi) = \mu_{Li,0} - e\varphi \quad (1)$$

where $\mu_{Li,0}$ is the chemical potential of lithium metal, e is the elementary charge, and φ is the potential referenced to a lithium metal anode. Python Materials Genomics (pymatgen)[37] code was used to construct the grand phase diagram, which provided the most stable compounds as a function of Li chemical potential.

The chemical reaction energy of the Li_3MCl_6 SEs was determined based on a method by Richards et al.[38] Four commercial cathode materials, namely, $LiCoO_2$ (LCO), $LiMn_2O_4$ (LMO), $LiFePO_4$ (LFP), and $Li(NiMnCo)_{1/3}O_2$ (NMC), were used to examine the chemical stability of the Li_3MCl_6 SEs against the cathode materials. The hydrolysis stability was evaluated using the chemical reaction energy between the Li_3MCl_6 SEs and H_2O. The chemical stability of the sulfide SEs (Li_6PS_5Cl, $Li_{10}GeP_2S_{12}$, and Li_3PS_4) against cathode materials and moisture were also calculated to compare the stability of the chloride and sulfide SEs.

The crystal structure of lithium chlorides Li_3MCl_6 was obtained using the data mined structure prediction (DMSP) algorithm by Hautier et al.,[39] which facilitated to generate a new and reasonable crystal structure by the chemical substitution of the existing materials.[37,40] After collecting the M_1–M_2–X ternary materials, the most reasonable space group was selected using the DMSP algorithm for lithium chlorides Li_3MCl_6.

BVSE calculations were performed to investigate the Li-ion migration path and the energy barriers in the Li_3MCl_6 SEs using the SoftBV software tool.[41,42] Li site energies ($E_{BVSE,Li}$) were calculated for a dense grid with a resolution of 0.1 Å using the Morse type SoftBV interaction potential. The Li migration path was identified based on the isosurface of $E_{BVSE,Li}$. The minimum value required to form a migration path was used as the energy barrier. The crystal structures and ionic migration path were visualized using the VESTA program.[43]

The Li-ion diffusivity within the Li_3MCl_6 SEs was calculated using AIMD calculations. Due to the demanding nature of AIMD calculations, a lower energy cutoff of 350 eV, gamma point-only sampling of the Brillouin zone, and the NVT ensemble with a Nosé–Hoover thermostat[44] were used. Mean squared displacement (MSD) data were collected for 80 ps at 600 and 700 K, and 40 ps at 800, 900, and 1000 K. The time step used for AIMD was 2 fs, and the MSD

https://dx.doi.org/10.1021/acsami.0c07003
ACS Appl. Mater. Interfaces 2020, 12, 34806–34814

values were measured after an equilibration time of 20 ps. The diffusion coefficient (D) was derived from the MSD of Li ions

$$D = \frac{1}{2dt}\langle[\mathbf{r}(t + t_0) - \mathbf{r}(t_0)]^2\rangle \quad (2)$$

where d is the dimensionality of the system, t_0 is the initial time, t is the time window for MSD, and the angled brackets indicate average overall Li ions. The ionic conductivity (σ) was calculated using the Nernst−Einstein equation

$$\sigma = \frac{(ze)^2 cD}{k_B T} \quad (3)$$

where z is the valence of an ion, e is the elementary charge, c is the concentration of the ion, D is the diffusion coefficient, k_B is the Boltzmann constant, and T is the temperature.

3. RESULTS

3.1. Structures and Phase Stability. The space group of A_3BX_6 (A^+, B^{3+}, and X^-) was examined for the structure prediction of the Li_3MCl_6 SEs using the DMSP algorithm. The DMSP algorithm suggested that the $C2$ (monoclinic), $P321$ (trigonal), and $Pna2_1$ (orthorhombic) space groups are the most appropriate candidates for the substitution. This prediction is in good agreement with the crystal structures of the Li_3MCl_6, exhibiting the trigonal ($P\bar{3}m1$) structure for Y, Tb, and Tm,[45,46] the orthorhombic ($Pnma$) structure for Y, Yb, and Lu,[46,47] and the monoclinic ($C2/m$) structure for Sc.[46] All of the Li_3MCl_6 was prepared using these three types of structures (total of 51 Li_3MCl_6 structures), as shown in Table 1. The crystal structures of Li_3ScCl_6 (monoclinic, mp-686004), Li_3ErCl_6 (trigonal, mp-676361), and Li_3AlF_6 (orthorhombic, mp-556020) in the MP[33] database were selected to generate the structure of Li_3MCl_6. After appropriate ionic substitution, the structures and ionic position of Li_3MCl_6 were fully relaxed. The lattice constants of Li_3MCl_6 for three space groups are presented in Table S1. The lattice constants of Li_3MCl_6 in Table S1 indicate that the fully relaxed Li_3MCl_6 structures maintained their symmetries.

The phase stability of the Li_3MCl_6 structures was determined using the E_{hull} of Li_3MCl_6 in the Li−M−Cl phase diagram, as listed in Table 1. The trend of the crystal structures of Li_3MCl_6 is consistent with the experimental results. The monoclinic Li_3ScCl_6 is found to be a stable phase compared to the trigonal and orthorhombic phases.[27,45] Experimentally synthesized trigonal Li_3MCl_6 (M = Tb, Dy, Ho, Er, and Tm)[45,46] and orthorhombic Li_3MCl_6 (M = Y, and Lu)[46,47] structures exhibit E_{hull} values below 25 meV/atom, confirming that the phase stability calculations are in good agreement with the experiments. The Li_3MCl_6 (M = Bi, Dy, Er, Ho, In, Lu, Sm, Tb, and Tm) are stable phases for all the space groups. Based on the E_{hull}, several Li_3MCl_6 (M = Al, Ga, La, Nd, and Sb) exceeded the stability criterion (>25 meV/atom), indicating that these compounds are unstable for all three space groups. The phase stability calculations exhibited the stable 12 Li_3MCl_6 (M = Bi, Dy, Er, Ho, In, Lu, Sc, Sm, Tb, Tl, Tm, and Y) phases.

Mostly, monoclinic Li_3MCl_6 structures exhibited the lowest total energy and E_{hull} among the three space groups, as shown in Table S2. However, the negligible energy difference (~10 meV/atom) among monoclinic, trigonal, and orthorhombic structures indicated that trigonal and orthorhombic structures could be stabilized at high temperature by the entropic effect. Based on the energy difference between monoclinic and trigonal structures in Figure S1, Li_3MCl_6 SEs with smaller ionic radii of M such as Sc (75 pm) and In (80 pm) are likely to maintain a monoclinic structure. In comparison, other Li_3MCl_6 SEs with larger ionic radii of M (>88 pm, Er, Y, Ho, Dy, Tb, Sm, and Bi) can exhibit trigonal phase at high temperature during syntheses procedures, which are consistent with experimental results.[21,27,45−47]

3.2. Electrochemical and Chemical Stabilities. The electrochemical and chemical stabilities of Li_3MCl_6 SEs were investigated using the most stable phases for each Li_3MCl_6 SE in Table 1. The electrochemical stability window was calculated based on the grand potential phase diagram as a function of Li chemical potential, as shown in Figure 1.

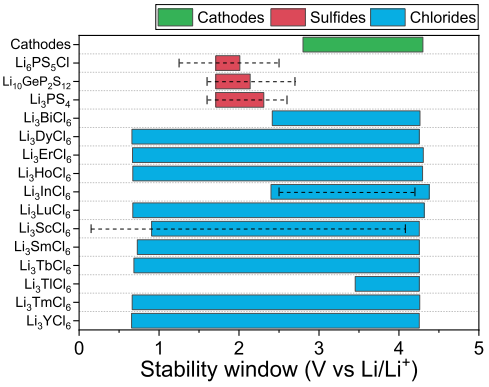

Figure 1. Electrochemical stability window of lithium chloride SEs (Li_3MCl_6) and lithium sulfide SEs (Li_6PS_5Cl, $Li_{10}GeP_2S_{12}$, and Li_3PS_4). The experimental results are presented for Li_6PS_5Cl, $Li_{10}GeP_2S_{12}$, Li_3PS_4, Li_3InCl_6, and Li_3ScCl_6 with a dashed line.

Theoretical electrochemical stability windows are in good agreement with the experimental results for Li_6PS_5Cl,[48] $Li_{10}GeP_2S_{12}$,[49] Li_3PS_4,[50] Li_3InCl_6,[25] and Li_3ScCl_6,[27] which are presented with a dashed line. The Li_3MCl_6 SEs exhibited a wide stability window compared to Li sulfide SEs (e.g., Li_6PS_5Cl, $Li_{10}GeP_2S_{12}$, and Li_3PS_4). The oxidation potential of the Li sulfide SEs was approximately 2 V, which indicated that the sulfide SEs were unstable against oxidation. However, the Li_3MCl_6 SEs generally exhibited a wide stability window and a high oxidation potential. All of the stable Li_3MCl_6 SEs exhibited an oxidation potential above 4.2 V, while the operation potential of typical cathode materials ranges between 2.8 and 4.3 V. Most of the Li_3MCl_6 SEs exhibited a wide stability window that covers this range, indicating that Li_3MCl_6 are stable SE candidates for applications with high-voltage cathodes. The reduction and oxidation potentials of the stable Li_3MCl_6 SEs are listed in Table S3. The reduction potential of Li_3TlCl_6 was higher than those of others (above 3 V) because of the decomposition to TlCl and LiCl phases, indicating that Li_3TlCl_6 is unstable and susceptible to reduction if used with typical cathode materials.

The reaction energies between the stable Li_3MCl_6 SEs and four commercial cathode materials, LCO, LMO, LFP, and NMC, were calculated as shown in Figure 2. The chemical reaction energy between Li_3MCl_6 and LMO was below 30 meV/atom, indicating the chemical stability of Li_3MCl_6 against the LMO cathode. The reaction energies were slightly higher for LFP (~40 meV/atom) and LCO (~50 meV/atom), but kinetics at the interface can hinder the decomposition of the Li_3MCl_6 SEs and the cathode material. The reaction energies for NMC were higher than those of other cathode materials

https://dx.doi.org/10.1021/acsami.0c07003
ACS Appl. Mater. Interfaces 2020, 12, 34806−34814

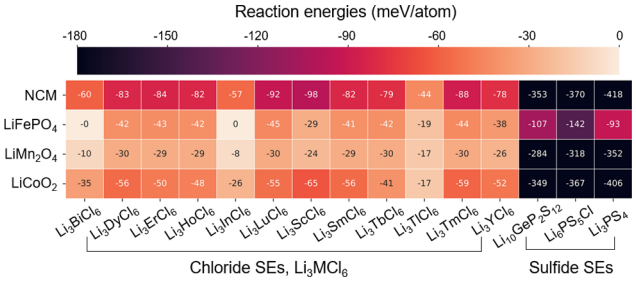

Figure 2. Heat map of the maximum reaction energy between 12 lithium chloride and three lithium sulfide SEs and four cathode materials (LCO, LMO, LFP, and NMC). The details of chemical reactions including decomposition phases between SEs and cathode materials are shown in Table S4.

(~80 meV/atom). The chemical reaction energy between the Li_3MCl_6 SEs and cathode materials was much lower (<100 meV/atom) than the sulfide SEs (above 300 meV/atom for NMC, LMO, and LCO), where phase decomposition was expected at the sulfide SE interface. The reaction energy between the sulfide SEs and the LFP cathode material was approximately 100 meV/atom, which would also result in chemical decomposition at the interface.

The reaction energies of chloride and sulfide SEs against the cathode materials are negative, suggesting that these are not stable against chemical decomposition (thermodynamically preferred reaction). However, the kinetic barrier can prevent the chemical reaction of chloride SEs due to the lower reaction energy (<100 meV/atom). The sulfide SEs can react with the cathode material, but the decomposition phase at the interface can hinder the further decomposition of sulfide SEs. The details of the decomposition reactions between the 12 stable Li_3MCl_6 (i.e., Li chloride) and three Li sulfide SEs and the four cathode materials are presented in Table S4.

The reaction energies between the Li_3MCl_6 and Li sulfide SEs and H_2O were calculated to determine hydrolysis stability, as listed in Table S4. All of the Li_3MCl_6 SEs exhibited excellent hydrolysis stability, and no decomposition phases were found. This confirms previous experimental results, which demonstrated the stability of Li_3InCl_6 after exposure to H_2O.[26] Exposure to humid air can result in the formation of hydrate Li_3MCl_6 phase based on the experimental results of Li_3InCl_6.[26] Nevertheless, the phase decomposition of Li_3MCl_6 would not occur, and the hydrate phase can be recovered to pristine SE after a drying step. The reaction energies between the sulfide SEs and H_2O were 50, 92, and 49 meV/atom for $Li_{10}GeP_2S_{12}$, Li_6PS_5Cl, and Li_3PS_4, respectively. This indicated that Li sulfide SEs reacted with H_2O and generated H_2S (Table S4), which was expected based on previous experimental results.[15]

The electrochemical stability window and chemical stability of the Li_3MCl_6 SEs against cathode materials and moisture demonstrated several advantages compared to the sulfide SEs. The high oxidation potential (>4.2 V) of the Li_3MCl_6 SEs was appropriate for use with high-voltage cathode materials, and the interfacial stability of the Li_3MCl_6 SEs against cathode materials such as LMO, LCO, and LFP was excellent. In addition, the hydrolysis stability of the Li_3MCl_6 SEs is expected to reduce the cost of the synthesis process. Conversely, the Li sulfide SEs had a narrow stability window and high chemical reaction energies against cathode materials, indicating that additional coatings are required to stabilize the interface between the Li sulfide SEs and cathode materials.[51,52]

3.3. Li-Ion Migration Pathways. The Li-ion migration path and energy barrier in the Li_3MCl_6 SEs were investigated using the BVSE method. The Li-ionic migration within the monoclinic, trigonal, and orthorhombic structures of the 12 stable Li_3MCl_6 SEs was examined. Calculation results from the BVSE indicated that Li-ion migration paths in monoclinic structures included a three-dimensional cross-layer and two-dimensional intralayer paths (Figure 3a), which were connected by tetrahedral interstitial sites between octahedral sites (Oct-Tet-Oct). The trigonal and orthorhombic structures (including hcp anion sublattice) exhibited anisotropic migration paths (Figure 3b,c; one-dimensional migration path along the *c*-axis between octahedral sites (Oct-Oct) and two-dimensional migration path along the *ab*-plane between octahedral sites via interstitial tetrahedral sites (Oct-Tet-Oct)).

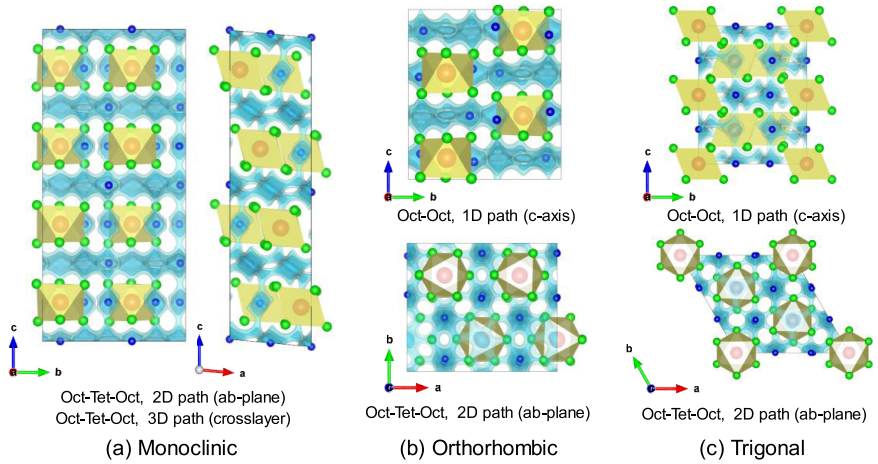

Figure 3. Li-ion migration pathway in (a) monoclinic, (b) orthorhombic, and (c) trigonal Li_3MCl_6 obtained using the BVSE method. Blue atom and yellow polyhedral correspond to Li and MCl_6, respectively, while isosurface with light blue corresponds to Li ion migration path. Monoclinic phase (ccp anion sublattice) exhibits two-dimensional intralayer and three-dimensional cross-layer paths between octahedral sites via tetrahedral interstitial sites (Oct-Tet-Oct), while trigonal and orthorhombic phase (hcp anion sublattice) exhibit anisotropic paths including a one-dimensional path along the *c*-axis between octahedral sites (Oct-Oct) and two-dimensional migration path along the *ab*-plane between octahedral sites via interstitial tetrahedral sites (Oct-Tet-Oct).

https://dx.doi.org/10.1021/acsami.0c07003
ACS Appl. Mater. Interfaces 2020, 12, 34806−34814

Details of the migration path are shown in Figure S2. These migration paths are in good agreement with previous works for Li_3YCl_6 (hcp anion sublattice) and Li_3YBr_6 (ccp anion sublattice).[20,22] Calculation results from the BVSE showed that Li_3MCl_6 SEs in the same space group exhibited identical ionic path, indicating that the transport properties of Li_3MCl_6 are dependent on the structures (i.e., space group) of Li_3MCl_6.

The energy barriers of Li-ion migration between the octahedral Li sites (from occupied Li site to empty Li site) were evaluated using the BVSE method for monoclinic, trigonal, and orthorhombic Li_3MCl_6 structures (total 36 structures). The migration energy barrier structures as a function of migration path (3D Oct-Tet-Oct path in monoclinic structure, and 1D Oct-Oct path/2D Oct-Tet-Oct path in orthorhombic and trigonal structures) were shown in Figure 4. Most Li_3MCl_6 showed a lower energy barrier of approximately 0.51 eV in monoclinic structures, while orthorhombic structures showed slightly higher energy barriers. The energy barriers of migration along the *c*-axis through face sharing octahedral sites (Oct-Oct) in orthorhombic were approximately 0.58 eV, and the energy barriers between octahedral sites via interstitial tetrahedral sites (Oct-Tet-Oct) along the two-dimensional *ab*-plane were about 0.57 eV. Trigonal structures exhibited higher energy barriers among the three space groups of Li_3MCl_6. The energy barriers of migration in trigonal structures were higher for 1D (Oct-Oct) and 2D (Oct-Tet-Oct) paths (0.59 and 0.75 eV, respectively). Figure 5 shows the energy barrier in monoclinic Li_3InCl_6 and orthorhombic and trigonal Li_3YCl_6 structures. The energy barrier for 12 Li_3MCl_6 in monoclinic, trigonal, and orthorhombic structures are presented in Figures S3−S5 and Table S5. Li-ion diffusivity could be increased in monoclinic and orthorhombic structures for Li_3MCl_6. Trigonal structures could exhibit sluggish Li-ion diffusivity compared to other structures. These results are in good agreement with the previous experimental works that monoclinic Li_3InCl_6 and Li_3ScCl_6 exhibit fast ionic conduction (2 and 3 mS/cm, respectively),[26,27] while trigonal Li_3YCl_6 and Li_3ErCl_6 show lower ionic conductivity (0.5 and 0.3 mS/cm, respectively).[22]

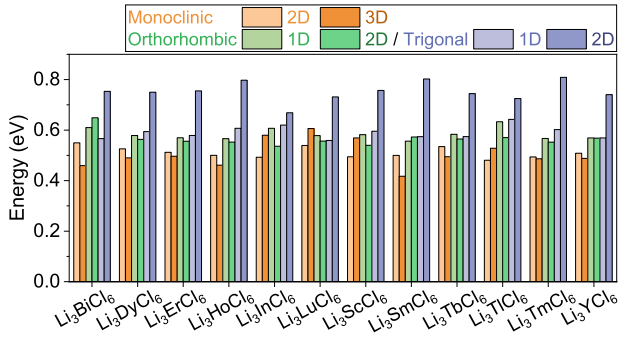

Figure 4. Li-ion migration energy barriers between octahedral Li sites along the 2D/3D Oct-Tet-Oct path in a monoclinic structure and the 1D Oct-Oct path and 2D Oct-Tet-Oct path in trigonal and orthorhombic Li_3MCl_6 structures from the BVSE calculations. The details of the energy barrier of 12 Li_3MCl_6 SEs for three space groups (total 36 structures) are presented in Figures S3−S5.

Although BVSE is a simplified empirical energy calculation that often overestimates activation energy, BVSE is known as an efficient screening method for analyzing the relative height of the migration barrier.[53] In addition, the isosurface of Li-ion densities from BVSE can provide insight into the existence of the possible Li-ion diffusion pathway in the candidate structures and the dimensionality of diffusion. The preliminary results done by BVSE motivate further quantitative analysis through AIMD, which requires considerable computational efforts.

3.4. Li-Ion Diffusivity. AIMD simulations calculations were performed to examine the Li-ion diffusivity and activation energy of Li_3MCl_6. Due to the demanding nature of AIMD, several elements with various ionic radii were used as M in Li_3MCl_6 in the AIMD calculations, including Sc (74.5 pm), In (80 pm), Lu (86 pm), and Y (90 pm). The diffusivity of Li ions in the Li_3MCl_6 SEs is illustrated by the Arrhenius plot given in Figure 6a, which indicates that the Li-ion diffusivity in monoclinic (M) Li_3InCl_6 and Li_3ScCl_6 is higher than that in orthorhombic (O) and trigonal (T) structures. Trigonal Li_3YCl_6 exhibited lower ionic diffusivity compared to that in orthorhombic Li_3YCl_6. The Li-ion MSD for the Arrhenius plot in Figure 6a is shown in Figure S6. The activation energy was 0.20, 0.21, 0.23, 0.24, and 0.26 for Li_3InCl_6 (M), Li_3ScCl_6 (M), Li_3LuCl_6 (O), Li_3YCl_6 (O), and Li_3YCl_6 (T), respectively, indicating that the monoclinic Li_3InCl_6 and Li_3ScCl_6 SEs exhibit fast ion diffusivity than other structures. These are in good agreement with the calculation results from the BVSE model in the previous section.

The fast ion migration along the intralayer in monoclinic Li_3InCl_6 and Li_3ScCl_6 from the BVSE model in Figure 4 was confirmed using the AIMD results in Figure 6b,c. The Li-ion diffusivity is higher in the *ab*-plane (intralayer) compared to

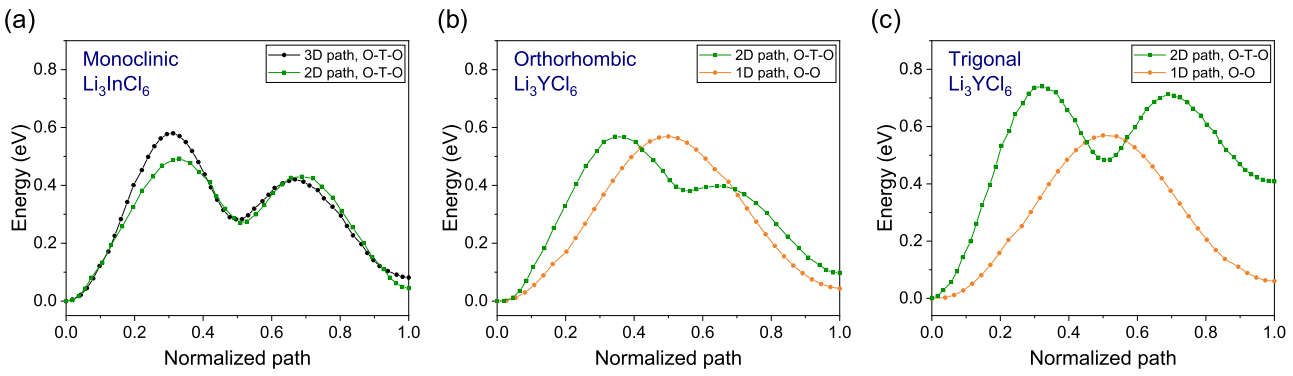

Figure 5. Li-ion migration energy barriers between octahedral Li sites along the (a) 2D and 3D Oct-Tet-Oct path in monoclinic Li_3InCl_6 and (b, c) 1D Oct-Oct path and 2D Oct-Tet-Oct path in (b) orthorhombic Li_3YCl_6 and (c) trigonal Li_3YCl_6 from the BVSE model.

https://dx.doi.org/10.1021/acsami.0c07003
ACS Appl. Mater. Interfaces 2020, 12, 34806−34814

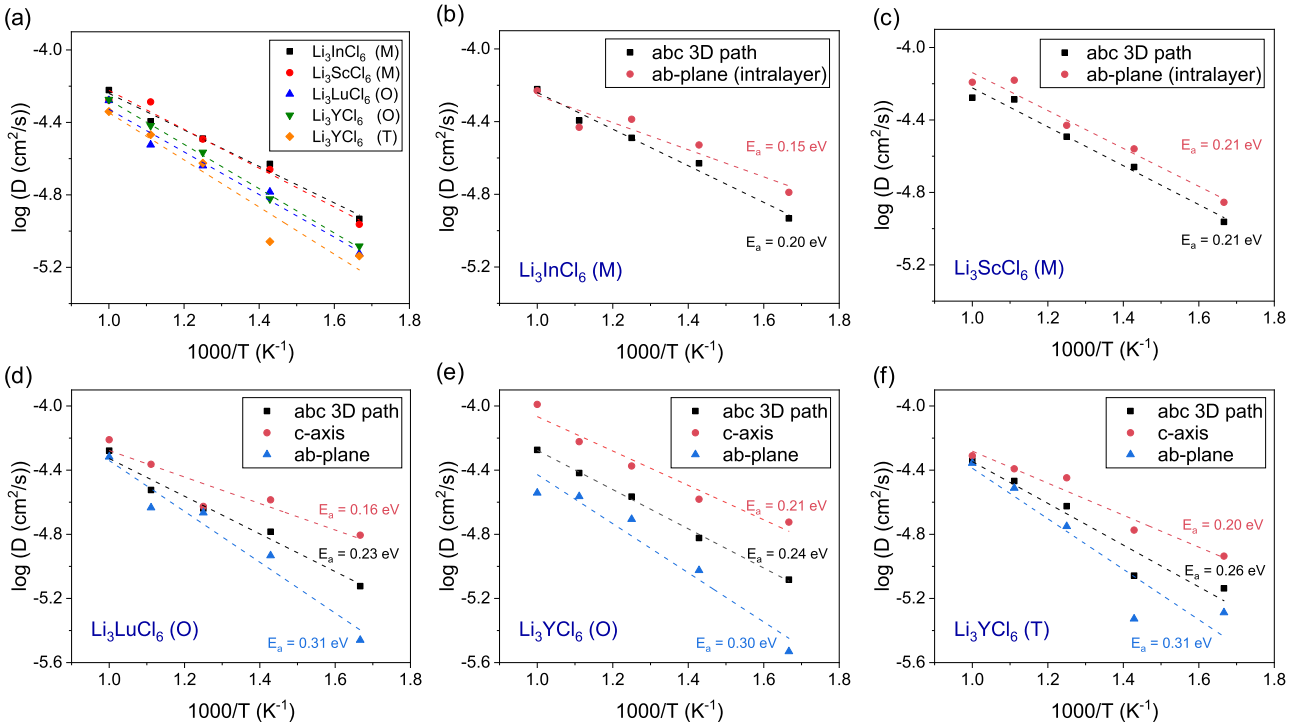

Figure 6. Arrhenius plots for (a) 3D Li-ion diffusivity in Li_3InCl_6, Li_3ScCl_6, Li_3LuCl_6, and Li_3YCl_6. Li-ion migration through the intralayer (*ab*-plane) 2D path are included in monoclinic (b) Li_3InCl_6 and (c) Li_3ScCl_6, while 1D (*c*-axis) and 2D (*ab*-plane) paths are included in orthorhombic (d) Li_3LuCl_6 and (e) Li_3YCl_6 and (f) trigonal Li_3YCl_6.

three-dimensional ion diffusion. Also, Li-ion migration along the *c*-axis (Oct-Oct) and the *ab*-plane (Oct-Tet-Oct) for orthorhombic Li_3LuCl_6 and Li_3YCl_6 and trigonal Li_3YCl_6 was examined using the AIMD calculations (Figure 6d–f). Li-ion migration along the *c*-axis (1D Oct-Oct path) showed higher ionic diffusivity, while Li-ion migration through the *ab*-plane (2D Oct-Tet-Oct) exhibited lower ionic diffusivity and higher activation energy for all Li_3LuCl_6 (O), Li_3YCl_6 (O), and Li_3YCl_6 (T) structures.

Based on the calculation results from the BVSE and AIMD, monoclinic Li_3MCl_6 structures exhibit fast ion migration, while orthorhombic and trigonal Li_3MCl_6 structures show lower ionic diffusivity due to sluggish ion migration along two-dimensional Oct-Tet-Oct path. According to the formation energy of the Li_3MCl_6 structures in three space groups as a function of the effective ionic radii of M (Table 1 and Figure S1) and ionic transport properties from the BVSE and AIMD, monoclinic Li_3InCl_6 and Li_3ScCl_6 structures exhibit higher ionic conductivities among Li_3MCl_6 SEs.

For the further enhancement of Li-ion migration in monoclinic Li_3InCl_6 and Li_3ScCl_6, the effects of Li vacancy on the transport properties were examined using the BVSE and AIMD calculations. Li vacancy was formed by the substitution of half M^{3+} with Zr^{4+} in Li_3MCl_6 SEs, resulting in $Li_{2.5}In_{0.5}Zr_{0.5}Cl_6$ and $Li_{2.5}Sc_{0.5}Zr_{0.5}Cl_6$. Both Zr-substituted Li_3MCl_6 (M = In and Sc) maintained the monoclinic symmetry, as shown in Table S6. The E_{hull} values from the phase stability calculations indicated that both structures are stable (E_{hull} < 25 meV/atom). The details of lattice constants and phase stability are shown in Table S6. $Li_{2.5}In_{0.5}Zr_{0.5}Cl_6$ and $Li_{2.5}Sc_{0.5}Zr_{0.5}Cl_6$ also showed a wide electrochemical stability window (2.50–4.31 and 1.72–4.26 V, respectively) and moderate chemical stability against cathode materials (reaction energy under 100 meV/atom) as shown in Table S7.

AIMD calculations were conducted to investigate the Li-ion diffusivity and activation energy of $Li_{2.5}In_{0.5}Zr_{0.5}Cl_6$ and $Li_{2.5}Sc_{0.5}Zr_{0.5}Cl_6$, as shown in Figures 7 and S7. The Zr-

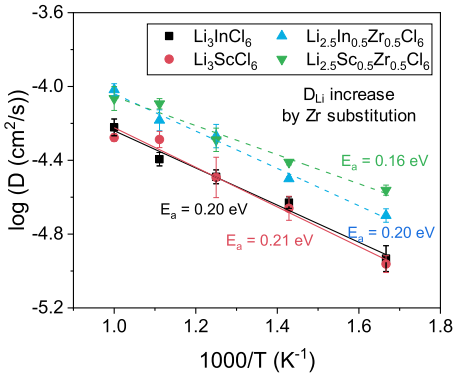

Figure 7. Arrhenius plots for Li-ion diffusivity in Li_3InCl_6, $Li_{2.5}In_{0.5}Zr_{0.5}Cl_6$, Li_3ScCl_6, and $Li_{2.5}Sc_{0.5}Zr_{0.5}Cl_6$.

substituted structures exhibited higher Li-ion diffusivity and lower activation energy. The ionic conductivity at room temperature was calculated by extrapolating the Arrhenius plots (Figure S8). The ionic conductivities of Li_3InCl_6 and Li_3ScCl_6 are in good agreement with previous works.[20,54,55] Zr-substituted Li_3MCl_6 structures increased the ionic conductivity to 27 and 89 for M = In and Sc, respectively (Table 2). This improved conductivity (up to fourfold) demonstrated the development of Zr-substituted Li_3MCl_6 superionic conductors. As Li vacancy by substitution further enhanced the ionic conductivity, the optimization of element type for substitution, such a Ti, Ge, Zr, Sn, Mo, Ce, Hf, W, and Pb, and the ratio of

https://dx.doi.org/10.1021/acsami.0c07003
ACS Appl. Mater. Interfaces 2020, 12, 34806–34814

Table 2. Li-Ion Conductivity at 300 K and Activation Energy of the Li_3InCl_6, Li_3ScCl_6, $Li_{2.5}In_{0.5}Zr_{0.5}Cl_6$, and $Li_{2.5}Sc_{0.5}Zr_{0.5}Cl_6$, from the AIMD Calculations[a]

composition	E_a (eV)	σ (mS/cm)	σ_{300K} (mS/cm)
Li_3InCl_6	0.20	21	2 (expt.)[26] 1.5 (expt.)[25] 6 (calc.)[54,55]
Li_3ScCl_6	0.21	16	29 (calc.)[20] 3.02 (expt.)[27]
$Li_{2.5}In_{0.5}Zr_{0.5}Cl_6$	0.20	27	
$Li_{2.5}Sc_{0.5}Zr_{0.5}Cl_6$	0.16	89	

[a]The ionic conductivities were extrapolated from the high-temperature values.

substitution (level of Li vacancy) in the Li_3MCl_6 SEs is recommended to develop superionic Li chloride SEs.

A recent theoretical study[56] shows that sodium halide SEs (Na_3YX_6, X = Cl, Br) are also promising SEs due to their high ionic conductivity, good chemical stability, and wide electrochemical window. Therefore, theoretical design works in this study can also be conducted to explore novel halide-based Na SEs (Na_3MX_6, X = Cl, Br, I). The Na-ion migration path and energy barrier could be identified based on their structures using the BVSE methods, which could be subsequently confirmed by AIMD simulations.

4. CONCLUSIONS

Several lithium chloride Li_3MCl_6 (M = In, Y, Er, and Sc) SEs have been reported as promising SEs due to their high ionic conductivity, wide electrochemical window, and chemical stability. Here, we systematically investigated 17 Li_3MCl_6 (M = Al, Bi, Dy, Er, Ga, Ho, In, La, Lu, Nd, Sb, Sc, Sm, Tb, Tl, Tm, and Y) to identify the novel and promising SEs. The phase stability calculations indicated that 12 Li_3MCl_6 (M = Bi, Dy, Er, Ho, In, Lu, Sc, Sm, Tb, Tl, Tm, and Y) were stable. The formation energy of Li_3MCl_6 suggested that Li_3MCl_6 SEs with smaller ionic radii of M such as Sc and In are likely to maintain monoclinic structures, while other Li_3MCl_6 SEs with larger ionic radii of M (Er, Y, Ho, Dy, Tb, Sm, and Bi) can exhibit a trigonal phase. The electrochemical stability window of the Li_3MCl_6 SEs (except Li_3TlCl_6) was wide and sufficient to cover the operation potential of typical cathode materials. Li_3MCl_6 SEs also exhibited good chemical stability against cathode materials and moisture, while sulfide SEs were predicted to be unstable.

In addition, Li-ion transport properties for monoclinic, trigonal, and orthorhombic Li_3MCl_6 SEs were investigated using the BVSE and AIMD. Li-ion migration paths were dependent on the structure of Li_3MCl_6. Most Li_3MCl_6 showed the lowest energy barrier in monoclinic structures, while orthorhombic structures showed slightly higher energy barriers. Trigonal structures exhibited the highest energy barriers among the three space groups. AIMD simulations were further performed to examine the Li-ion diffusivity of Li_3MCl_6. AIMD results showed the fast ion migration along the intralayer in monoclinic structures and the 1D path along the *c*-axis in orthorhombic and trigonal structures. Li-ion migration through the 2D path along the *ab*-plane exhibited lower ionic diffusivity and higher activation energy in orthorhombic and trigonal structures. According to the formation energy of Li_3MCl_6 structures and ionic transport properties, monoclinic Li_3InCl_6 and Li_3ScCl_6 structures exhibit the highest ionic conductivities among Li_3MCl_6 SEs. Further enhancement of ionic conductivity in monoclinic Li_3InCl_6 and Li_3ScCl_6 was achieved by the aliovalent substitution of M^{3+} with Zr^{4+} forming Li vacancy. AIMD calculations showed the increase of ionic conductivity (up to fourfold at 300 K) for $Li_{2.5}In_{0.5}Zr_{0.5}Cl_6$ and $Li_{2.5}Sc_{0.5}Zr_{0.5}Cl_6$. As Li vacancy was predicted to improve the ionic conductivity, the optimization of substitution in the Li_3MCl_6 SEs is suggested to develop superionic Li chloride SEs.

■ ASSOCIATED CONTENT

Supporting Information

The Supporting Information is available free of charge at https://pubs.acs.org/doi/10.1021/acsami.0c07003.

Lattice parameters, formation energy, chemical reactions, Li-ion migration path, migration energy barriers, and Li-ion MSD for monoclinic, orthorhombic, and trigonal Li_3MCl_6 SEs (PDF)

■ AUTHOR INFORMATION

Corresponding Author

Seungho Yu − *Center for Energy Storage Research, Korea Institute of Science and Technology, Seoul 02792, Republic of Korea;* orcid.org/0000-0003-3912-6463; Email: shyu@kist.re.kr

Authors

Dongsu Park − *Center for Energy Storage Research, Korea Institute of Science and Technology, Seoul 02792, Republic of Korea; School of Mechanical Engineering, Korea University, Seoul 02841, Republic of Korea*

Haesun Park − *Materials Science Division and Joint Center for Energy Storage Research (JCESR), Argonne National Laboratory, Lemont, Illinois 60439, United States;* orcid.org/0000-0001-6266-8151

Yongheum Lee − *Center for Energy Storage Research, Korea Institute of Science and Technology, Seoul 02792, Republic of Korea; Division of Energy & Environment Technology, KIST School, Korea University of Science and Technology, Seoul 02792, Republic of Korea*

Sang-Ok Kim − *Center for Energy Storage Research, Korea Institute of Science and Technology, Seoul 02792, Republic of Korea; Division of Energy & Environment Technology, KIST School, Korea University of Science and Technology, Seoul 02792, Republic of Korea;* orcid.org/0000-0001-5628-9331

Hun-Gi Jung − *Center for Energy Storage Research, Korea Institute of Science and Technology, Seoul 02792, Republic of Korea; Division of Energy & Environment Technology, KIST School, Korea University of Science and Technology, Seoul 02792, Republic of Korea;* orcid.org/0000-0002-2162-2680

Kyung Yoon Chung − *Center for Energy Storage Research, Korea Institute of Science and Technology, Seoul 02792, Republic of Korea; Division of Energy & Environment Technology, KIST School, Korea University of Science and Technology, Seoul 02792, Republic of Korea;* orcid.org/0000-0002-1273-746X

https://dx.doi.org/10.1021/acsami.0c07003
ACS Appl. Mater. Interfaces 2020, 12, 34806−34814

Joon Hyung Shim − *School of Mechanical Engineering, Korea University, Seoul 02841, Republic of Korea;* orcid.org/0000-0002-3995-1968

Complete contact information is available at: https://pubs.acs.org/10.1021/acsami.0c07003

Notes

The authors declare no competing financial interest.

■ ACKNOWLEDGMENTS

This research was supported by the Technology Development Program to Solve Climate Changes of the National Research Foundation (NRF) funded by the Ministry of Science & ICT of Korea (2017M1A2A2044482), by the Development Program of Core Industrial Technology funded by the Ministry of Trade, Industry & Energy of Korea (No. 20007045), and by the institutional program of the Korea Institute of Science and Technology (Project No. 2E30202). Work by H.P. was supported as part of the Joint Center for Energy Storage Research, an Energy Innovation Hub funded by the U.S. Department of Energy, Office of Science, Basic Energy Sciences.

■ REFERENCES

(1) Larcher, D.; Tarascon, J. M. Towards Greener and More Sustainable Batteries for Electrical Energy Storage. *Nat. Chem.* **2015**, *7*, 19−29.

(2) Tarascon, J. M.; Armand, M. Issues and Challenges Facing Rechargeable Lithium Batteries. *Nature* **2001**, *414*, 359−367.

(3) Li, J.; Ma, C.; Chi, M.; Liang, C.; Dudney, N. J. Solid Electrolyte: the Key for High-Voltage Lithium Batteries. *Adv. Energy Mater.* **2015**, *5*, No. 1401408.

(4) Manthiram, A.; Yu, X.; Wang, S. Lithium Battery Chemistries Enabled by Solid-State Electrolytes. *Nat. Rev. Mater.* **2017**, *2*, No. 16103.

(5) Sun, C.; Liu, J.; Gong, Y.; Wilkinson, D. P.; Zhang, J. Recent Advances in All-Solid-State Rechargeable Lithium Batteries. *Nano Energy* **2017**, *33*, 363−386.

(6) Albertus, P.; Babinec, S.; Litzelman, S.; Newman, A. Status and Challenges in Enabling the Lithium Metal Electrode for High-Energy and Low-Cost Rechargeable Batteries. *Nat. Energy* **2018**, *3*, 16−21.

(7) Liu, Y.; He, P.; Zhou, H. Rechargeable Solid-State Li−Air and Li−S Batteries: Materials, Construction, and Challenges. *Adv. Energy Mater.* **2018**, *8*, No. 1701602.

(8) Lin, D.; Liu, Y.; Cui, Y. Reviving the Lithium Metal Anode for High-Energy Batteries. *Nat. Nanotechnol.* **2017**, *12*, 194−206.

(9) Goodenough, J. B.; Kim, Y. Challenges for Rechargeable Li Batteries. *Chem. Mater.* **2010**, *22*, 587−603.

(10) Kim, S.; Oguchi, H.; Toyama, N.; Sato, T.; Takagi, S.; Otomo, T.; Arunkumar, D.; Kuwata, N.; Kawamura, J.; Orimo, S.-i. A Complex Hydride Lithium Superionic Conductor for High-Energy-Density All-Solid-State Lithium Metal Batteries. *Nat. Commun.* **2019**, *10*, No. 1081.

(11) Cuan, J.; Zhou, Y.; Zhou, T.; Ling, S.; Rui, K.; Guo, Z.; Liu, H.; Yu, X. Borohydride-Scaffolded Li/Na/Mg Fast Ionic Conductors for Promising Solid-State Electrolytes. *Adv. Mater.* **2019**, *31*, No. 1803533.

(12) Kato, Y.; Hori, S.; Saito, T.; Suzuki, K.; Hirayama, M.; Mitsui, A.; Yonemura, M.; Iba, H.; Kanno, R. High-Power All-Solid-State Batteries Using Sulfide Superionic Conductors. *Nat. Energy* **2016**, *1*, No. 16030.

(13) Kamaya, N.; Homma, K.; Yamakawa, Y.; Hirayama, M.; Kanno, R.; Yonemura, M.; Kamiyama, T.; Kato, Y.; Hama, S.; Kawamoto, K.; Mitsui, A. A Lithium Superionic Conductor. *Nat. Mater.* **2011**, *10*, 682−686.

(14) Zhu, Y.; He, X.; Mo, Y. Origin of Outstanding Stability in the Lithium Solid Electrolyte Materials: Insights from Thermodynamic Analyses Based on First-Principles Calculations. *ACS Appl. Mater. Interfaces* **2015**, *7*, 23685−23693.

(15) Muramatsu, H.; Hayashi, A.; Ohtomo, T.; Hama, S.; Tatsumisago, M. Structural Change of Li2S-P2S5 Sulfide Solid Electrolytes in the Atmosphere. *Solid State Ionics* **2011**, *182*, 116−119.

(16) Murugan, R.; Thangadurai, V.; Weppner, W. Fast Lithium Ion Conduction in Garnet-Type Li7La3Zr2O12. *Angew. Chem., Int. Ed.* **2007**, *46*, 7778−7781.

(17) Allen, J. L.; Wolfenstine, J.; Rangasamy, E.; Sakamoto, J. Effect of Substitution (Ta, Al, Ga) on the Conductivity of Li7La3Zr2O12. *J. Power Sources* **2012**, *206*, 315−319.

(18) Wang, D.; Sun, Q.; Luo, J.; Liang, J.; Sun, Y.; Li, R.; Adair, K.; Zhang, L.; Yang, R.; Lu, S.; Huang, H.; Sun, X. Mitigating the Interfacial Degradation in Cathodes for High-Performance Oxide-Based Solid-State Lithium Batteries. *ACS Appl. Mater. Interfaces* **2019**, *11*, 4954−4961.

(19) Liu, Y. L.; Sun, Q.; Wang, D. W.; Adair, K.; Liang, J. N.; Sun, X. L. Development of the Cold Sintering Process and Its Application in Solid-State Lithium Batteries. *J. Power Sources* **2018**, *393*, 193−203.

(20) Wang, S.; Bai, Q.; Nolan, A. M.; Liu, Y.; Gong, S.; Sun, Q.; Mo, Y. Lithium Chlorides and Bromides as Promising Solid-State Chemistries for Fast Ion Conductors with Good Electrochemical Stability. *Angew. Chem., Int. Ed.* **2019**, *58*, 8039−8043.

(21) Li, X.; Liang, J.; Yang, X.; Adair, K. R.; Wang, C.; Zhao, F.; Sun, X. Progress and Perspectives on Halide Lithium Conductors for All-Solid-State Lithium Batteries. *Energy Environ. Sci.* **2020**, *13*, 1429−1461.

(22) Asano, T.; Sakai, A.; Ouchi, S.; Sakaida, M.; Miyazaki, A.; Hasegawa, S. Solid Halide Electrolytes with High Lithium-Ion Conductivity for Application in 4 V Class Bulk-Type All-Solid-State Batteries. *Adv. Mater.* **2018**, *30*, No. 1803075.

(23) Muy, S.; Voss, J.; Schlem, R.; Koerver, R.; Sedlmaier, S. J.; Maglia, F.; Lamp, P.; Zeier, W. G.; Shao-Horn, Y. High-Throughput Screening of Solid-State Li-Ion Conductors Using Lattice-Dynamics Descriptors. *iScience* **2019**, *16*, 270−282.

(24) Schlem, R.; Muy, S.; Prinz, N.; Banik, A.; Shao-Horn, Y.; Zobel, M.; Zeier, W. G. Mechanochemical Synthesis: A Tool to Tune Cation Site Disorder and Ionic Transport Properties of Li3MCl6 (M = Y, Er) Superionic Conductors. *Adv. Energy Mater.* **2020**, *10*, No. 1903719.

(25) Li, X.; Liang, J.; Luo, J.; Norouzi Banis, M.; Wang, C.; Li, W.; Deng, S.; Yu, C.; Zhao, F.; Hu, Y.; Sham, T.-K.; Zhang, L.; Zhao, S.; Lu, S.; Huang, H.; Li, R.; Adair, K. R.; Sun, X. Air-Stable Li3InCl6 Electrolyte with High Voltage Compatibility for All-Solid-State Batteries. *Energy Environ. Sci.* **2019**, *12*, 2665−2671.

(26) Li, X.; Liang, J.; Chen, N.; Luo, J.; Adair, K. R.; Wang, C.; Banis, M. N.; Sham, T.-K.; Zhang, L.; Zhao, S.; Lu, S.; Huang, H.; Li, R.; Sun, X. Water-Mediated Synthesis of a Superionic Halide Solid Electrolyte. *Angew. Chem., Int. Ed.* **2019**, *58*, 16427−16432.

(27) Liang, J.; Li, X.; Wang, S.; Adair, K. R.; Li, W.; Zhao, Y.; Wang, C.; Hu, Y.; Zhang, L.; Zhao, S.; Lu, S.; Huang, H.; Li, R.; Mo, Y.; Sun, X. Site-Occupation-Tuned Superionic LixScCl3+x Halide Solid Electrolytes for All-Solid-State Batteries. *J. Am. Chem. Soc.* **2020**, *142*, 7012−7022.

(28) Park, K.-H.; Kaup, K.; Assoud, A.; Zhang, Q.; Wu, X.; Nazar, L. F. High-Voltage Superionic Halide Solid Electrolytes for All-Solid-State Li-Ion Batteries. *ACS Energy Lett.* **2020**, *5*, 533−539.

(29) Blöchl, P. E. Projector Augmented-Wave Method. *Phys. Rev. B* **1994**, *50*, 17953−17979.

(30) Perdew, J. P.; Burke, K.; Ernzerhof, M. Generalized Gradient Approximation Made Simple. *Phys. Rev. Lett.* **1996**, *77*, 3865−3868.

(31) Kresse, G.; Furthmüller, J. Efficient Iterative Schemes for Ab Initio Total-Energy Calculations Using a Plane-Wave Basis Set. *Phys. Rev. B* **1996**, *54*, 11169−11186.

(32) Kresse, G.; Joubert, D. From Ultrasoft Pseudopotentials to the Projector Augmented-Wave Method. *Phys. Rev. B* **1999**, *59*, 1758−1775.

(33) Jain, A.; Ong, S. P.; Hautier, G.; Chen, W.; Richards, W. D.; Dacek, S.; Cholia, S.; Gunter, D.; Skinner, D.; Ceder, G.; Persson, K. A. Commentary: The Materials Project: A Materials Genome Approach to Accelerating Materials Innovation. *APL Mater.* **2013**, *1*, No. 011002.
(34) Wang, L.; Maxisch, T.; Ceder, G. Oxidation Energies of Transition Metal Oxides within the GGA+*U* Framework. *Phys. Rev. B* **2006**, *73*, No. 195107.
(35) Jain, A.; Hautier, G.; Ong, S. P.; Moore, C. J.; Fischer, C. C.; Persson, K. A.; Ceder, G. Formation Enthalpies by Mixing GGA and GGA+*U* Calculations. *Phys. Rev. B* **2011**, *84*, No. 045115.
(36) Ong, S. P.; Wang, L.; Kang, B.; Ceder, G. Li−Fe−P−O2 Phase Diagram from First Principles Calculations. *Chem. Mater.* **2008**, *20*, 1798−1807.
(37) Ong, S. P.; Richards, W. D.; Jain, A.; Hautier, G.; Kocher, M.; Cholia, S.; Gunter, D.; Chevrier, V. L.; Persson, K. A.; Ceder, G. Python Materials Genomics (Pymatgen): A Robust, Open-Source Python Library for Materials Analysis. *Comput. Mater. Sci.* **2013**, *68*, 314−319.
(38) Richards, W. D.; Miara, L. J.; Wang, Y.; Kim, J. C.; Ceder, G. Interface Stability in Solid-State Batteries. *Chem. Mater.* **2016**, *28*, 266−273.
(39) Hautier, G.; Fischer, C.; Ehrlacher, V.; Jain, A.; Ceder, G. Data Mined Ionic Substitutions for the Discovery of New Compounds. *Inorg. Chem.* **2011**, *50*, 656−663.
(40) Sun, W.; Bartel, C. J.; Arca, E.; Bauers, S. R.; Matthews, B.; Orvañanos, B.; Chen, B.-R.; Toney, M. F.; Schelhas, L. T.; Tumas, W.; Tate, J.; Zakutayev, A.; Lany, S.; Holder, A. M.; Ceder, G. A Map of the Inorganic Ternary Metal Nitrides. *Nat. Mater.* **2019**, *18*, 732−739.
(41) Chen, H.; Adams, S. Bond Softness Sensitive Bond-Valence Parameters for Crystal Structure Plausibility Tests. *IUCrJ* **2017**, *4*, 614−625.
(42) Chen, H.; Wong, L. L.; Adams, S. SoftBV - a Software Tool for Screening the Materials Genome of Inorganic Fast Ion Conductors. *Acta Crystallogr., Sect. B: Struct. Sci., Cryst. Eng. Mater.* **2019**, *75*, 18−33.
(43) Momma, K.; Izumi, F. VESTA 3 for Three-Dimensional Visualization of Crystal, Volumetric and Morphology Data. *J. Appl. Crystallogr.* **2011**, *44*, 1272−1276.
(44) Nosé, S. A Unified Formulation of the Constant Temperature Molecular Dynamics Methods. *J. Chem. Phys.* **1984**, *81*, 511−519.
(45) Altorfer, F. Investigations into the Fast Ionic Conductors γ-CuBr, Li2S, Na2S, Ba2NH, NaTaN2 and Li3HoCl6 by means of Neutron Scattering. *Eidgenoessische Technische Hochschule* 1994, LNS-171.
(46) Bohnsack, A.; Stenzel, F.; Zajonc, A.; Balzer, G.; Wickleder, M. S.; Meyer, G. Ternäre Halogenide vom Typ A3MX6. VI [1]. Ternäre Chloride der Selten-Erd-Elemente mit Lithium, Li3MCl6 (M = Tb, Lu, Y, Sc): Synthese, Kristallstrukturen und Ionenbewegung. *Z. Anorg. Allg. Chem.* **1997**, *623*, 1067−1073.
(47) Steiner, H.-J.; Lutz, H. D. Neue Schnelle Ionenleiter vom Typ MMIIICl6 (MI = Li, Na, Ag; MIII = In, Y). *Z. Anorg. Allg. Chem.* **1992**, *613*, 26−30.
(48) Schwietert, T. K.; Arszelewska, V. A.; Wang, C.; Yu, C.; Vasileiadis, A.; de Klerk, N. J.; Hageman, J.; Hupfer, T.; Kerkamm, I.; Xu, Y.; et al. Clarifying the Relationship between Redox Activity and Electrochemical Stability in Solid Electrolytes. *Nat. Mater.* **2020**, *19*, 428−435.
(49) Han, F.; Gao, T.; Zhu, Y.; Gaskell, K. J.; Wang, C. A Battery Made from a Single Material. *Adv. Mater.* **2015**, *27*, 3473−3483.
(50) Hakari, T.; Nagao, M.; Hayashi, A.; Tatsumisago, M. All-Solid-State Lithium Batteries with Li3PS4 Glass as Active Material. *J. Power Sources* **2015**, *293*, 721−725.
(51) Yu, S.; Park, H.; Siegel, D. J. Thermodynamic Assessment of Coating Materials for Solid-State Li, Na, and K Batteries. *ACS Appl. Mater. Interfaces* **2019**, *11*, 36607−36615.
(52) Xiao, Y.; Miara, L. J.; Wang, Y.; Ceder, G. Computational Screening of Cathode Coatings for Solid-State Batteries. *Joule* **2019**, *3*, 1252−1275.
(53) Xiao, R.; Li, H.; Chen, L. High-Throughput Design and Optimization of Fast Lithium Ion Conductors by the Combination of Bond-Valence Method and Density Functional Theory. *Sci. Rep.* **2015**, *5*, No. 14227.
(54) Zevgolis, A.; Wood, B. C.; Mehmedović, Z.; Hall, A. T.; Alves, T. C.; Adelstein, N. Alloying Effects on Superionic Conductivity in Lithium Indium Halides for All-Solid-State Batteries. *APL Mater.* **2018**, *6*, No. 047903.
(55) Sendek, A. D.; Cubuk, E. D.; Antoniuk, E. R.; Cheon, G.; Cui, Y.; Reed, E. J. Machine Learning-Assisted Discovery of Solid Li-Ion Conducting Materials. *Chem. Mater.* **2019**, *31*, 342−352.
(56) Qie, Y.; Wang, S.; Fu, S.; Xie, H.; Sun, Q.; Jena, P. Yttrium−Sodium Halides as Promising Solid-State Electrolytes with High Ionic Conductivity and Stability for Na-Ion Batteries. *J. Phys. Chem. Lett.* **2020**, *11*, 3376−3383.

https://dx.doi.org/10.1021/acsami.0c07003
ACS Appl. Mater. Interfaces 2020, 12, 34806−34814